# Thermodynamic Budget Diagrams for the Hurricane Subcloud Layer

ALAN K. BETTS*
*West Pawlet, VT 05775*

JOANNE SIMPSON
*Laboratory for Atmospheres, NASA/Goddard Space Flight Center, Greenbelt, MD 20771*

(Manuscript received 19 May 1986, in final form 12 September 1986)

ABSTRACT

We reexamine the idealized hurricane boundary layer budget from Malkus and Riehl using vector diagrams for the thermodynamic budgets in the light of recent observational studies. We conclude that a large air–sea temperature difference can only be maintained with both large fluxes through cloud-base level and a large evaporative cooling of the subcloud layer. The high $\theta_E$ values observed in hurricane eyewalls can be reached if these cloud-base and evaporative fluxes are reduced and the subcloud layer moves toward the sea surface virtual potential temperature.

## 1. Introduction

The magnitude and role of sea–air fluxes in tropical storms are crucial issues which have been repeatedly discussed with conflicting results for more than thirty years. One thread has been the question of the importance of CISK, the cooperative linear instability mechanism originally proposed by Ooyama (1964) and Charney and Eliassen (1964), and later reviewed in Ooyama (1982). Ooyama (1969) extended his work to show how the convection and surface fluxes in a mature cyclone are controlled by the dynamics of the balanced flow. Emanuel (1986) has, in contrast, recently emphasized the view of the mature hurricane as a Carnot-type heat engine driven by a finite amplitude air–sea interaction instability. Many models of storm development, however, (see Anthes, 1982) rely on the release of CAPE (Convective Available Potential Energy), while the nonlinear model of Carrier et al. (1971) is completely dependent on CAPE, explicitly asserting that no increases in sea–air fluxes in the storm core are required compared with the undisturbed tropical environment.

Here, we consider an important link in the resolution of these differences, namely how we may estimate the sea–air sensible and latent heat fluxes, what their range of magnitudes can be under different assumed or observed conditions, and how the fluxes may vary spatially and temporally. These conditions lead to questions regarding mechanisms and suggest important foci for future investigations.

The main difficulty in discriminating the degree of validity of widely different approaches to the hurricane problem, all of which are sensitive to the lower boundary conditions, is observational. Direct measurements in violent winds close to a storm-roughened sea surface distorted by huge waves and often obscured by flying spray are virtually impossible and therefore rarely exist. Accurate remote measurements at the interface, while increasingly feasible, are expensive and still rare, particularly within a data base complete enough to calculate fluxes either by turbulent transfer formulations or even by the bulk equations, which also require a drag coefficient. Data to obtain the latter are not yet available in hurricane-force winds.

Because of these formidable observational difficulties, all estimates of sea–air fluxes in strong oceanic cyclones have involved compositing, extrapolation, or interpolation with fragmentary data samples, often fitted together with models or budget calculations. The models and budget calculations nearly always relate to the storm scale of motion, which is much larger than convective or turbulent scales. Models are fraught with untestable assumptions which often require neglect of potentially vital variations. In budget calculations, the desired fluxes are commonly relatively small residual differences between large opposing terms. Thus, it is not surprising that published estimates of sea–air sensible and latent heat fluxes and their ratio (the so-called Bowen ratio) have differed greatly with the method and data used; controversies focused upon which estimates are "right" are presently not likely to be constructive, as we will elucidate further.

To advance understanding and encourage productive future storm boundary layer experiments, we reas-

* Visiting Scientist, Laboratory for Atmospheres, NASA/Goddard Space Flight Center, Greenbelt, MD 20771.

sess a well-known study resulting from the pioneering efforts of the National Hurricane Research Project (NHRP) in light of recent developments.

Malkus and Riehl (1960, called MR herein) evolved a model for the inflow layer of a steady state mature hurricane. To address the thermodynamics, they developed an empirical relation, from data in the NHRP archives, between core pressure drop $\delta p$ (in mb relative to the mean tropical environment) and the increase in equivalent potential temperature $\delta\theta_E$ (in °C) of the ascending air in the penetrative convective towers of the core, namely

$$\delta p \sim -2.5\delta\theta_E. \quad (1)$$

The high cloud towers were postulated to be ascending nearly undiluted with the increased $\theta_E$ at their bases provided by sea–air fluxes. MR were the first in a 20-year series of attempts to test their hypothesis concerning the role of "hot towers" and related ocean fluxes and to explore its implications (see Anthes, 1982). To apportion the low-level increase in $\theta_E$ between sensible and latent fluxes, they used earlier observations (Byers, 1944; Riehl, 1954) of a roughly isothermal subcloud layer as the air experiences rapidly falling pressure during inflow; they also assumed a constant (warmer) sea temperature. With these assumptions, the estimated core ($r \leqslant 90$ km) sensible and latent fluxes came out about factors of 50 and 12, respectively, higher than sea–air fluxes over the undisturbed tropical ocean. Their calculated Bowen ratio was about 0.4 compared with then current estimates of 0.05 to 0.1 for the trade wind region. Recycling of inflow air by means of rain-cooled downdrafts was suggested by MR as the mechanism of sensible heat augmentation, as the same authors had suggested[1] to explain a comparably large estimate of the Bowen ratio from a budget study of the equatorial trough zone (Riehl and Malkus, 1958). In the hurricane core, air slightly cooler than that of moist adiabatic ascent is found at middle to low levels. These departures make a negligible difference to the relationship in Eq. (1), but are believed essential in the downdraft mechanism.

Garstang's careful shipboard measurements in a weak-wind trade disturbance (discussed by Malkus, 1962) derived a Bowen ratio of 0.1, due mainly to cool unsaturated downdrafts. In MR, the greatly enhanced sea–air fluxes were consistent with bulk formulae using normal trade wind values of the drag coefficient. High wind speeds, together with a larger than normal sea–air property difference, were adequate for the estimated flux enhancement.

These concepts and assumptions were first tested in an observationally based budget analysis of Hurricane Daisy 1958 (Riehl and Malkus, 1961). The National Hurricane Research Project (NHRP) flew multi-aircraft patterns through the storm core on three successive days from intensification to maturity. Support for enhanced oceanic fluxes and a Bowen ratio roughly half the magnitude of MR were found, with direct sea temperature measurements available only on the intensifying day. Even higher fluxes were observationally deduced from NHRP data during the 1960s (Hawkins and Rubsam, 1968; Hawkins and Imembo, 1976).

These high estimations of sea–air fluxes, particularly that of sensible heat, were challenged by numerical models and different observational approaches in the 1970s. Model results with a careful formulation of the boundary layer (Anthes and Chang, 1978) showed that the isothermal subcloud layer could be maintained by downward turbulent transfer. Frank (1977a,b) composited rawinsonde data from 143 Pacific typhoons and deduced a total flux that was about half that of MR, or comparable to that of Riehl and Malkus (1961) for the mature Daisy. Assuming no sensible heat flux through cloud base, he deduced a sensible heat flux of only 20%–25% that of MR, contributing to his assertion that their core values of $\theta_E$ were too high. Fendell (1974), using the Carrier closed-system analytic model, rejects increased fluxes and hence increased $\theta_E$ in the storm core, and so must call upon an outward-sloping eyewall for the crucial pressure gradient forces.

Calculation of $\theta_E$ from high-level (10.6 km) aircraft observations comparable to those of MR have been calculated by Riehl (1963). More recently, Rodgers et al. (1983) obtained similar $\theta_E$ values in the highest towers of Frederic (1979) by a combination of satellite and conventional observations.

By the mid-1980s, the improved aircraft data sets with updated instrumentation included three storms which also had some boundary layer and ocean measurements, namely Atlantic Hurricanes Frederic 1979 (Powell, 1982; Frank, 1984), Floyd 1981 (Barnes et al., 1983), and Australian Tropical Cyclone Kerry (Black et al., 1987; Holland and Black, 1987). Betts (1982) developed saturation point thermodynamics, which is here applied to the hurricane inflow, and Emanuel (1986) derived theoretically an equation similar to (1) based on less stringent assumptions. Under Emanuel's conditions,[2] the coefficient multiplying $\delta\theta$ is about 25%–30% higher than that in Eq. (1), relaxing somewhat the requirement for "excessive" $\theta_E$ over large portions of the core.

The purpose of this article is to reexamine the MR boundary layer budget in light of these developments

[1] In a later budget reassessment of the equatorial trough zone (Riehl and Simpson, 1979) using improved radiation, cloud, and oceanic transport data and including more realistic unsaturated downdrafts, the same authors calculated a smaller but still enhanced (relative to the trade wind region) Bowen ratio of 0.2.

[2] Emanuel's assumptions are an axisymmetric, steady storm with moist adiabatic ascent in the eyewall and an outflow temperature which corresponds to neutral buoyancy with respect to the far environment.

and of the increased recognition of the role of convective up- and downdraft circulations, evaporation of precipitation, and storm asymmetries to see what insight can be gained into the constraints upon both surface and cloud-base fluxes.

## 2. Subcloud layer budget equation

We shall present an idealized budget of a well-mixed subcloud layer using the vector thermodynamic notation of Betts (1983, 1984), and model data for the hurricane inflow layer adapted from MR. The advantage of this vector notation using air parcel saturation point (SP) is that all the static thermodynamic budgets can be visualized on one figure (e.g., Fig. 1). MR considered the inflow of a boundary layer air parcel from 90 to 30 km radius in a steady state hurricane (MR, Table 5). We shall construct a mean budget for this mean trajectory in the subcloud layer.

The Lagrangian budget for the subcloud layer mean SP can be written

$$\Delta p_B \dot{\mathbf{B}} = \omega_0(\mathbf{O}-\mathbf{B}) + \omega^{**}(\mathbf{B}^+ - \mathbf{B}) + \mathbf{E}. \quad (2)$$

Figure 1 shows some of the notation as well as two vector budgets (see sections 3 and 4). In (2), $\dot{\mathbf{B}}$ is the Lagrangian derivative for the subcloud mean saturation point. The terms on the right-hand side of (2) are the surface fluxes, the vertical advection and transports through the cloud-base level, and an evaporation term. Radiative effects are neglected. The surface flux $\omega_0$ $(\mathbf{O} - \mathbf{B})$ is parameterized in terms of a difference between the saturation points of the ocean surface $(\mathbf{O})$ and that of the mixed subcloud layer $(\mathbf{B})$ and a velocity scale $\omega_0 = \rho g C_0 V_0$ where $V_0$ is a surface wind speed and $C_0$ a corresponding bulk surface transfer coefficient (which we assume is the same for all the thermodynamic fields). At cloud base, we parameterize the thermodynamic fluxes as the product of a $p$-velocity scale $\omega^{**}$ and a difference $(\mathbf{B}^+ - \mathbf{B})$ between the mean subcloud layer and the environmental air at cloud-base level. The velocity scale $\omega^{**}$ can be expressed as a sum of terms

$$\omega^{**} = \omega^* + \bar{\omega} + \Delta\dot{p}_B, \quad (3)$$

where $\omega^*$, $\bar{\omega}$, and $\Delta\dot{p}_B$ are the contributions from the convective circulation (including updrafts and downdrafts), the mean circulation, and the change of mixed layer depth respectively (Betts, 1973). We might expect in a hurricane $\Delta\dot{p}_B$ to be negligible compared to the first two terms in Eq. (3), and the budget analysis in which we shall estimate $\omega^{**}$ will confirm this. Betts (1976) showed how the effect of evaporatively driven downdrafts could be split into the sum of a vertical advection and an evaporation term. The term $\mathbf{E}$ represents evaporation in the subcloud layer. There are two contributions to this, which we cannot separate: the evaporation of falling precipitation and the evaporation of ocean spray. We shall assume that these processes conserve $\theta_E$ while changing the subcloud layer saturation level ($p^*$), and parameterize this term as

$$\mathbf{E} = \omega_E \boldsymbol{\Gamma}_w \Delta p_B, \quad (4)$$

where $\boldsymbol{\Gamma}_w$ is the moist adiabat (constant $\theta_E$) and $\omega_E$ is a $p$-velocity scale representing the tendency of saturation level due to the evaporation process, and $\Delta p_B$ is the pressure thickness of the subcloud layer. Although the evaporation of ocean spray may make a significant contribution to the vector $\mathbf{E}$, the combination of the two terms we have represented as cloud-base fluxes and evaporation are probably dominated by the effect of moist updrafts and evaporatively driven downdrafts through cloud-base level.

A final transformation, which will be used, is to reexpress the cloud base jump

$$\mathbf{B}^+ - \mathbf{B} = \boldsymbol{\Gamma}\mathcal{P}_B, \quad (5)$$

where $\boldsymbol{\Gamma}$ is gradient of SP near cloud base, and $\mathcal{P}_B = p^* - p$ the saturation pressure departure of the environment at cloud base. Equation (2) then becomes

$$\Delta p_B \dot{\mathbf{B}} = \omega_0(\mathbf{O}-\mathbf{B}) + \omega^{**}\boldsymbol{\Gamma}\mathcal{P}_B + \omega_E \boldsymbol{\Gamma}_w \Delta p_B. \quad (6)$$

We shall now construct vector diagrams showing possible balances between the terms of (6).

## 3. Malkus and Riehl (1960)

Malkus and Riehl (1960) examined the budget of the hurricane inflow layer. We shall take their model data, and assumptions, and reproduce a subcloud layer budget. Their data will give the Lagrangian derivative, $\Delta\mathbf{p}_B\dot{B}$, and surface flux term for a mean trajectory from 90 to 30 km toward the hurricane eyewall. We shall show these do not balance in the subcloud layer and estimate the magnitudes of the cloud-base flux and the subcloud evaporation flux vectors. Additional information on the vector $\boldsymbol{\Gamma}$ is needed to separate cloud-base and evaporation fluxes, and we shall use data from a composite by Frank (1977a). The vector $\boldsymbol{\Gamma}_w$ is that of the moist adiabat and is known.

Table 1a shows a reconstruction of the thermodynamic endpoints of a trajectory from 90 to 30 km radius in MR, Table 5, using more accurate formulae for equivalent potential temperature (Simpson, 1978; Bolton, 1980). The ocean temperature was taken as 28°C and an air–sea temperature difference of 2°C was assumed. A relative humidity of 84% at 90 km radius (assumed outside the storm circulation) was taken from Jordan's (1958) hurricane season mean sounding. A hydrostatic computation was used to relate surface pressure fall and $\theta_E$ rise in the rain area (assuming a moist adiabatic structure from surface to 100 mb and no height variation at 100 mb). With $\theta_E$ recomputed, this is

$$-\delta P_s \sim 3\delta\theta_E$$

TABLE 1. (a) Data adapted from Malkus and Riehl (1960, Table 5): hurricane subcloud layer inflow between 90 and 30 km radius. (b) Air data adjusted to have same $\theta_v$ as the ocean.

| | $r$ (km) | $p_0$ (mb) | $\theta_E$ (K) | $T$ (°C) | $q$ (g kg$^{-1}$) | $\theta$ (K) | $\theta_v$ (K) | $T^*$ (°C) | $p^*$ (mb) | $\Delta p_B$ (mb) |
|---|---|---|---|---|---|---|---|---|---|---|
| | | | | | (a) | | | | | |
| Air | | | | | | | | | | |
| $\mathbf{B}_1$ | 90 | 996 | 353.2 | 26 | 18.25 | 299.50 | 302.8 | 22.49 | 955.7 | 40.3 |
| $\mathbf{B}_2$ | 30 | 966 | 363.2 | 26 | 20.49 | 302.12 | 305.9 | 24.17 | 945.5 | 20.5 |
| Ocean | | | | | | | | | | |
| $\mathbf{O}_1$ | 90 | 996 | 374.8 | 28 | 24.54 | 301.50 | 306.0 | 28 | 996 | |
| $\mathbf{O}_2$ | 30 | 966 | 380.8 | 28 | 25.34 | 304.14 | 308.9 | 28 | 996 | |
| | | | | | (b) | | | | | |
| $\mathbf{B}'_1$ | 90 | 996 | 365.8 | 28.6 | 21.37 | 302.07 | 306.0 | 25.03 | 955.7 | 40.3 |
| $\mathbf{B}'_2$ | 30 | 966 | 375.7 | 28.3 | 23.60 | 304.46 | 308.9 | 26.47 | 945.5 | 20.5 |

for values of $\theta_E$ near 360 K. Emanuel (1986) has given new theoretical support for this relationship. Equation (6) will be scaled by $\frac{1}{2}\omega_0$ (the factor $\frac{1}{2}$ is arbitrary and was included simply to reduce the size of the vector diagram on Fig. 1), and $\dot{B}$ replaced by a finite difference over the whole trajectory, giving

$$\frac{\Delta p_B}{\Delta t}\frac{\Delta \mathbf{B}}{2\omega_0} = \frac{\mathbf{O}-\mathbf{B}}{2} + \frac{\omega^{**}\Gamma \mathcal{P}_B}{2\omega_0} + \frac{\omega_E \Gamma_w \Delta p_B}{2\omega_0}. \quad (7)$$

Table 2 shows the other parameters needed for the budget, and how they were determined. At wind speeds $\sim$50 m s$^{-1}$, the surface transfer coefficient is not well known; we used the same value as Emanuel (1986).

Figure 1 (solid lines) shows the vector components of the budget, and Table 3a the coordinates of the SPs on Fig. 1. It was constructed as follows. The **O** and **B** are midpoints of the vectors $\mathbf{O}_1\mathbf{O}_2$ and $\mathbf{B}_1\mathbf{B}_2$ in Table 1a. BC is the vector (**O** − **B**)/2. (All vectors are computed and plotted using $\theta$, $q$ as coordinate axes.) CD is the vector

$$-\frac{1}{2\omega_0}\frac{\Delta p_B}{\Delta t}\Delta \mathbf{B} = -0.143(\mathbf{B}_2 - \mathbf{B}_1).$$

The two remaining terms must have resultant **BD**. This vector represents an absolutely unstable stratification, and clearly could not represent simply the cloud-base flux term for which we expect $\Gamma$ to be between dry and moist adiabats (in fact, probably between dry and moist virtual adiabats; Betts, 1982). This means that the evaporation vector cannot be small. Its direction is known (that of the moist adiabat), so that if we know the direction of $\Gamma$ [associated with the vector $\mathbf{BB}^+$ through Eq. (5)], the vector diagram can be closed. For this idealized model, we shall choose a single value of $\Gamma$ from the tropical cyclone composite in Frank (1977a). His composite at a radius of $\sim$70 km gives a slope for $\Gamma$ of $(\partial\bar{\theta}/\partial p, \partial\bar{q}/\partial p) = (-3.84, 3.2)$(K/100 mb, g kg$^{-1}$/100 mb) between 950 and 900 mb. We shall construct Fig. 1 using the gradient $\partial\bar{\theta}/\partial\bar{q} = -1.20$ K/g kg$^{-1}$ along **BF** to preserve the coupling of the heat and moisture fluxes at cloud base.

The quadrilateral **BCDF** on Fig. 1 shows us the relative magnitude and direction of the components of the subcloud layer budget. It expresses the layer tendency as the sum of three vector components. We may rewrite (7) as

TABLE 2. Budget input parameters.

| | | | |
|---|---|---|---|
| $V_0$ | 50 | (m s$^{-1}$) | From Malkus and Riehl (1960) |
| $C_0$ | $2\times10^{-3}$ | | Estimated surface transfer coefficient |
| $\omega_0$ | 40.0 | (mb h$^{-1}$) | $=\rho g C_0 V_0$ |
| $\Delta p_B$ | 30.4 | (mb) | Mean depth of subcloud layer (Table 1) |
| $\Delta t$ | 2.67 | (h) | Inflow time from 90–30 km radius (Malkus and Riehl, 1960) |
| $\Delta\mathbf{B}$ | (2.62, 2.24) | (K, g kg$^{-1}$) | Vector for cloud-base tendency; from Table 1a |
| $\Delta\mathbf{B}'$ | (2.39, 2.23) | (K, g kg$^{-1}$) | Vector for cloud-base tendency; from Table 1b |
| $\bar{\Gamma}$ | (−3.84, 3.2) | (K/100 mb, g kg$^{-1}$/100 mb) | $(\partial\bar{\theta}/\partial p, \partial\bar{q}/\partial p)$ at cloud base from Frank (1977a); 0.7° radius, 950–900 mb average data |
| $\mathcal{P}_B$ | −18 | mb | From Frank (1977a) |

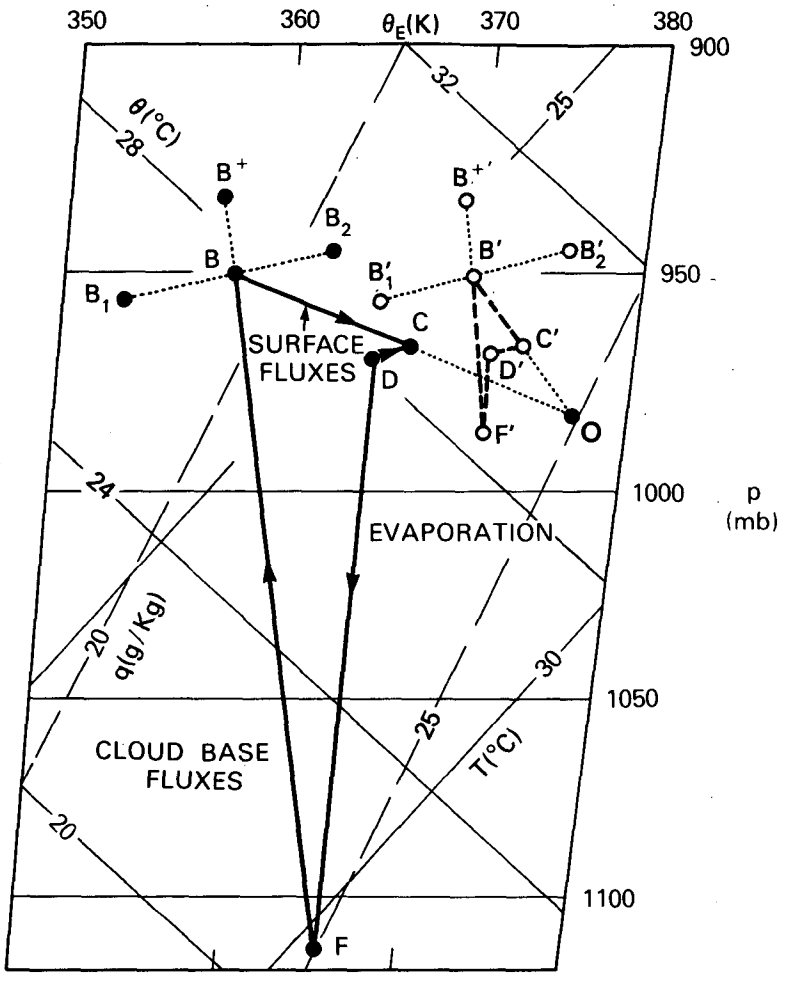


FIG. 1. Vector diagrams for the hurricane subcloud layer thermodynamic budget on a low-level tephigram. Solid lines are for Malkus and Riehl (1960) budget, dashed lines for modified budget with no air–sea $\theta_v$ difference. **O**, **B** are the saturation points of the ocean surface and the mixed subcloud layer for the mid-point of the inflow trajectory. The vectors **BC**, **FB** and **DF** represent the contributions to the subcloud layer budget of the ocean surface fluxes, the fluxes of heat and moisture through the level of cloud base and the evaporation of precipitation into the subcloud layer. The vector **DC** is the resultant Lagrangian time derivative for the subcloud layer. (See text for other symbols and a discussion of the scaling of the figure.)

$$\underset{\text{tendency}}{(\mathbf{C}-\mathbf{D})} = \underset{\text{surface fluxes}}{(\mathbf{C}-\mathbf{B})} + \underset{\text{cloud-base fluxes}}{(\mathbf{B}-\mathbf{F})} + \underset{\text{evaporation flux}}{(\mathbf{F}-\mathbf{D})}. \tag{8}$$

Because $(\mathbf{C}-\mathbf{D}) \ll (\mathbf{C}-\mathbf{B})$, we can conclude that no balance is possible without considering cloud-base and evaporation fluxes. We see that the derived cloud-base and evaporation fluxes are very large, much larger than the surface fluxes. The sum of these terms (cloud-base and evaporation fluxes) is the vector **BD**. This is the result of the large transports through cloud-base level due to moist updrafts and evaporatively driven downdrafts, the recycling proposed by Riehl and Malkus (1958) and MR. The effect of the evaporation process is to convert the vector $(\mathbf{B}-\mathbf{F})$, which represents warm, dry advection into the vector $\mathbf{B}-\mathbf{D}$, which is equivalent to the advection of cool, dry air into the subcloud layer (Betts, 1976). We shall find in section 4 that, if the subcloud layer has a warmer virtual potential temperature, less recycling is needed.

A major component of the vector $\mathbf{C}-\mathbf{B}$, which represents the surface fluxes, is of course the evaporation from the ocean surface. Its vector orientation is very different from $\mathbf{F}-\mathbf{D}$, which represents the evaporation of precipitation and ocean spray simply because the evaporation at the surface takes the latent heat from the ocean not the air.

Table 4a gives the four terms in (8), both as the SP differences on Fig. 1 and scaled to give sensible and latent heat fluxes in W $m^{-2}$. The surface fluxes are large, as might be expected with a surface wind speed of 50 m $s^{-1}$ and a surface transfer coefficient of $2.10^{-3}$.

TABLE 3. (a) Parameters in subcloud layer budget diagrams based on Tables 1a and 2. (b) Parameters in subcloud layer budget diagrams based on Tables 1b and 2: $\theta_v(\mathbf{B}') = \theta_v(\mathbf{O}) = 307.4$ K.

| | $T^*$ (°C) | $p^*$ (mb) | $\theta$ (K) | $q$ (g kg$^{-1}$) | $\theta_E$ (K) | $\theta_v$ (K) |
|---|---|---|---|---|---|---|
| | | | (a) | | | |
| **B** | 23.35 | 950.9 | 300.80 | 19.37 | 358.1 | |
| **C** | 25.80 | 967.4 | 301.80 | 22.15 | 367.8 | |
| **D** | 25.60 | 969.3 | 301.43 | 21.83 | 366.4 | |
| **F** | 30.21 | 1115.0 | 294.07 | 24.98 | 366.4 | |
| **O** | 28.0 | 981.0 | 302.81 | 24.93 | 377.7 | 307.4 |
| | | | (b) | | | |
| **B'** | 25.76 | 950.9 | 303.25 | 22.47 | 370.6 | 307.4 |
| **C'** | 26.88 | 965.8 | 303.03 | 23.70 | 374.2 | 307.4 |
| **D'** | 26.69 | 967.9 | 302.66 | 23.38 | 372.7 | 307.0 |
| **F'** | 27.30 | 986.1 | 301.64 | 23.80 | 372.7 | 306.0 |

However, the derived cloud-base and evaporation fluxes are even larger. They are major terms of the budget which cannot be neglected. Different assumptions on $\bar{\Gamma}$ (which we took from Frank, 1977a) will affect the mean magnitude of these terms somewhat (both are reduced as $\bar{\Gamma}$ becomes more unstable), but their magnitudes are still very large for plausible values of $\bar{\Gamma}$.

Table 4a also reexpresses the $p^*$ (saturation level) budget in terms of the tendency (in mb h$^{-1}$) for the subcloud layer associated with each of the four terms in (8). Cloud base rises very little ($\sim -5$ mb h$^{-1}$) despite very large opposing tendencies. The surface flux tendency would reduce cloud base at a rate of 43 mb h$^{-1}$; the cloud-base flux would lift cloud base at 432 mb h$^{-1}$, while evaporation into the subcloud layer would lower cloud base at a rate of 383 mb h$^{-1}$.

Table 4a gives an estimate of the cloud-base parameter $\omega^{**} \sim 730$ mb h$^{-1}$. This too is very large; we can estimate the cloud-base convective mass circulation from (3)

$$\omega^* = \omega^{**} - \bar{\omega} - \Delta\dot{p}_B.$$

From Table 1, $\Delta\dot{p}_B \sim -7$ mb h$^{-1}$ and, at cloud base, $\bar{\omega} \sim -31$ mb h$^{-1}$ (Table 2; found by integrating the convergence in MR through the mean subcloud layer thickness of 30.4 mb), so that $\omega^* \sim 768$ mb h$^{-1}$. We conclude that the vertical exchange at *cloud base* associated with updrafts and downdrafts, represented by $\omega^*$ and estimated from the thermodynamic budget, is more than an order of magnitude larger than the mean vertical motion, $\bar{\omega}$, estimated in MR from mass convergence. We note that Gray (1973) reached similar conclusions from the study of cloud cluster budgets.

Figure 1 was constructed using $\theta$ and $q$ as coordinates and the $\theta$, $q$ budgets are satisfied exactly. The derived $p^*$ budget involves some slight approximation (Betts, 1982, 1983): for example, Tables 4a and 4b give $-5$, $-6$ mb h$^{-1}$ for the residual $\dot{p}^*$, whereas Tables 1 and 2 give $-4$ mb h$^{-1}$. The size and location of the vector quadrilateral in Fig. 1 are arbitrary. The vectors represent tendencies, which have been plotted as SP differences using a velocity scale which was chosen as $\omega_0/2$ in Eq. (7). If we had chosen $\omega_0/4$, for example, and again started the figure at **B**, then the vectors **BF** and **BC** are halved to give a correspondingly smaller vector diagram.

## 4. No surface virtual heat flux

The results in section 3 are based on the budget of MR. One of their assumptions was that an air–sea temperature difference of 2°C was maintained along the trajectory into the hurricane. How can this be maintained in the face of a large upward sensible heat flux from the ocean and a large downward convective heat flux at cloud base? In the budget in Tables 3a and 4a, a subcloud layer cooler than the ocean is maintained by the large evaporation in the subcloud layer. We can illustrate this further by constructing a second vector budget, based on a different assumption on the air–sea temperature difference. We shall assume no air–sea difference in virtual potential temperature ($\theta_v$), but otherwise we shall keep ocean surface temperature and pressure, wind speed, and level of cloud base the same as in section 3. This changes $\theta_v$ of the subcloud layer, but not its mean relative humidity, and moves **B** to **B'** on Fig. 1. The dashed quadrilateral, and Tables 1b, 3b and 4b show the new budget. All the flux terms are reduced if the subcloud layer has the same $\theta_v$ as the ocean, and the evaporation and cloud-base fluxes are particularly reduced. Table 4b shows that the surface latent heat flux is halved; the surface sensible heat flux becomes small and negative (as is expected for zero $\theta_v$

TABLE 4. (a) Components of thermodynamic budget (Malkus and Riehl, 1960) from Table 3a. (b) Components of thermodynamic budget from Table 3b.

| Component | C-D tendency | C-B surface | B-F cloud base | F-D evaporation |
|---|---|---|---|---|
| | | (a) | | |
| $\Delta\theta$ (K) | 0.37 | 1.0 | 6.73 | −7.36 |
| $F_{c_p\theta}$ (W m$^{-2}$) | | 228 | 1535 | −1678 |
| $\Delta q$ (g kg$^{-1}$) | 0.32 | 2.78 | −5.61 | 3.15 |
| $F_{L_q}$ (W m$^{-2}$) | | 1578 | −3184 | 1788 |
| $\Delta p^*$ (mb) | −2 | 17 | −164 | 146 |
| $\dot{p}^*$ (mb h$^{-1}$) | −5 | 43 | −432 | 383 |
| $\omega_E$ (mb h$^{-1}$) | | | | 383 |
| $\omega^{**}$ (mb h$^{-1}$) | | | 730 | |
| $\omega^*$ (mb h$^{-1}$) | | | 768 | |
| | | (b) | | |
| $\Delta\theta$ (K) | 0.37 | −0.22 | 1.60 | −1.01 |
| $F_{c_p\theta}$ (W m$^{-2}$) | | −50 | 365 | −230 |
| $\Delta q$ (g kg$^{-1}$) | 0.32 | 1.23 | −1.33 | 0.42 |
| $F_{L_q}$ (W m$^{-2}$) | | 698 | −755 | 238 |
| $\Delta p^*$ (mb) | −2 | 15 | −35 | 18 |
| $\dot{p}^*$ (mb) | −6 | 39 | −93 | 48 |
| $\omega_E$ (mb h$^{-1}$) | | | | 48 |
| $\omega^{**}$ (mb h$^{-1}$) | | | 157 | |
| $\omega^*$ (mb h$^{-1}$) | | | 195 | |

flux), while the evaporation flux is only 14% of its earlier value (Table 4a). The cloud-base mass flux $\omega^* \sim 195$ mb $h^{-1}$, though greatly reduced, is still much larger than $\bar{\omega}$ and $\Delta p_B$. This dramatic change in the budget is associated with the change in $\theta_v$ of the mean subcloud layer from **B** to **B′**, which has become warmer and moister (at constant relative humidity). In contrast, changing subcloud relative humidity at constant $\theta_v$ or $\theta$ produces a much smaller reduction in the cloud-base fluxes (not shown).

## 5. Discussion

We shall now discuss several topics that were raised in the Introduction in light of the two budgets shown in Fig. 1.

### *a. Budget interpretation*

The budget represented by the solid lines in Fig. 1 suggests that a large air–sea temperature difference can only be maintained with both large cloud-base fluxes and a large evaporative cooling in the subcloud layer. This is likely to represent the budget of regions with strong precipitation-driven downdrafts. The second budget (dashed in Fig. 1), with no air–sea $\theta_v$ difference, may represent the balance in regions of a hurricane where the cloud-base and evaporation fluxes are much weaker, so that the subcloud layer becomes warmer and moister. This $\theta_v$ neutral structure can be considered a useful reference, because a much more stable structure [$\theta_v(\mathbf{B}') > \theta_v(\mathbf{O})$] would tend to reduce the surface latent heat flux, and convection out of the subcloud layer would be reduced.

### *b. Surface fluxes*

The surface fluxes for the two budgets differ significantly, but the observed range for different regions of a hurricane is also considerable. In a recent study of Hurricane Kerry, Black et al. (1987) show a spatial variation of the latent heat flux (inside 1° radius, but outside the eye) from 1100 to 1800 W $m^{-2}$ and a variation of the sensible heat flux from −60 to +60 W $m^{-2}$. Significant portions of Hurricane Kerry had a negative air–sea temperature difference, partly due to cold surface temperatures in the wake of the hurricane, and the downward heat flux in those regions was comparable to the value of −50 W $m^{-2}$ in Table 4b. However, both of our budgets used the same sea-surface temperature of 28°C. No regions of Hurricane Kerry showed upward sensible heat fluxes as large as the 230 W $m^{-2}$ in Table 4a, but the corresponding latent heat flux of 1600 W $m^{-2}$ is within the observed range for this hurricane.

It is clear that the Bowen ratio can have a large horizontal variation in a hurricane and a single average value might be misleading. Early studies of disturbed regions in the tropics (Malkus, 1962) showed that values of the Bowen ratio as high as 10% were observed (by Garstang, unpublished) in an easterly wave disturbance. Studies in GATE (GATE, 1977) showed Bowen Ratios $\geq 0.2$ at the leading edge of mesoscale convective systems. The value of 14% for the evaporation-cooled subcloud layer (Table 4a) seems consistent with these estimates, but clearly we need more measurements of the surface fluxes in hurricanes.

Rodgers et al. (1983) report satellite-derived values of the eyewall $\theta_E$ as high as 375 K in Hurricane Frederic and 387 K in Hurricane Allen, although the accuracy of these estimates is uncertain. Frank (1984) presented a composite analysis of Hurricane Frederic. His composite data (kindly supplied by the author) show a maximum radial mean $\theta_E$ of 368 K just inside the eyewall at the lowest aircraft flight level of 560 m. This mean value is a little lower than the estimate of Rodgers et al. (1983), derived from the maximum observed cloud-top heights. Jorgensen (1984) reports maximum eyewall values of $\theta_E$ for Hurricane Allen of 375 K, and values in the range 355–365 K outside the radius of maximum wind. Table 1a corresponds to the lower range of values of $\theta_E$ (maximum 363 K at $\mathbf{B}_2$). If the subcloud layer $\theta_v$ becomes as high as that of the ocean, then subcloud $\theta_E$ increases as high as 375 K at $\mathbf{B}'_2$ (Table 1b). This suggests that the very high $\theta_E$ values measured or estimated for the eyewall require that some of the subcloud layer air becomes as warm as the ocean.

### *c. High $\theta_E$ air*

It has long been recognized that the intensity of a hurricane is related to the highest $\theta_E$ values reached in the eyewall (MR), and the work of Emanuel (1986) confirms this. Our two prototype budgets show that higher $\theta_E$ values in the subcloud layer are reached if a positive air–sea temperature difference is not maintained, even though the surface fluxes are then reduced in magnitude. This is not as paradoxical as it seems at first. The lower subcloud $\theta_E$ ($\mathbf{B}_1\mathbf{B}\mathbf{B}_2$, in Fig. 1) is maintained by the strong cloud-base fluxes and subcloud evaporation; that is by the cooling and downward $\theta_E$ transport associated primarily with evaporatively driven downdrafts. In turn, this recycling both increases the surface fluxes and distributes them through an inflow layer that is deeper than the subcloud layer. If this recycling is reduced, the subcloud layer moves toward a higher mean $\theta_v$ and $\theta_E$, while the surface fluxes are reduced (and at the same time distributed through a shallower inflow layer). We conclude that although downdrafts increase the surface fluxes, they may reduce the increase of $\theta_E$ in the inflow, so that the details of the structure and intensity of a hurricane may well be related to the distribution of boundary layer cooling by downdrafts.

### *d. Fluxes across cloud-base level*

MR neglected vertical fluxes through 900 mb and Frank (1977b) assumed no sensible heat flux across cloud base. The estimates in Table 4 show that neither

of these are acceptable assumptions. The cloud-base transports can be very large and the thermodynamic budget of the hurricane boundary layer must consider both these, and the evaporation of both precipitation and spray in the subcloud layer. Since the recycling or cloud-base transports are large, a deep inflow layer (considerably deeper than the shallow subcloud layer) can be modified by the surface fluxes. However, we have shown that the highest subcloud layer $\theta_E$ values will be reached in those regions of the hurricane where the cooling and recycling of low $\theta_E$ air in evaporatively driven downdrafts, and consequently the air–sea temperature difference, are both reduced.

## 6. Conclusions

In conclusion, we have shown that vector thermodynamic diagrams can give insight into the coupling of processes in the hurricane subcloud layer. The examples we present based on the mean hurricane inflow analysis of MR are certainly highly simplified. More realistic trajectory analyses using recent aircraft data in asymmetric hurricanes are needed to extend the work further.

Comparison of the two budgets in Fig. 1 shows that a large air–sea temperature difference can only be maintained with large cloud-base fluxes and subcloud layer evaporative cooling. With this large cloud-base recycling, the subcloud $\theta_E$ remains low. The high $\theta_E$ values estimated for hurricane eyewalls ($\sim$375 K) can only be achieved if the cloud-base fluxes and evaporative cooling are much weaker, so that the subcloud layer moves to a higher $\theta_v$ (even as warm as the ocean), even though the surface fluxes are then reduced.

*Acknowledgments.* This work was supported by NASA/Goddard Space Flight Center under Contract NAS5-28800 and the National Science Foundation under Grant ATM8403333. The authors thank Ms. Kelly Wilson at Goddard for typing the manuscript.

## REFERENCES

Anthes, R. A., 1982: *Tropical Cyclones: Their Evolution, Structure and Effect. Meteor. Monogr.*, No. 41, Amer. Meteor. Soc., 207 pp.

——, and S. W. Chang, 1978: Response of the hurricane boundary layer to changes of sea surface temperature in a numerical model. *J. Atmos. Sci.*, **35**, 1240–1255.

Barnes, G. M., E. J. Zipser, D. Jorgensen and F. Marks, 1983: Mesoscale and convective scale structure of a hurricane rainband. *J. Atmos. Sci.*, **40**, 2125–2137.

Betts, A. K., 1973: Non-precipitating cumulus convection and its parameterization. *Quart. J. Roy. Meteor. Soc.*, **99**, 178–196.

——, 1976: The thermodynamic transformation of the tropical subcloud layer by precipitation and downdrafts. *J. Atmos. Sci.*, **33**, 1008–1020.

——, 1982: Saturation point analysis of moist convective overturning. *J. Atmos. Sci.*, **39**, 1484–1505.

——, 1983: Thermodynamics of mixed stratocumulus layers. *J. Atmos. Sci.*, **40**, 2655–2670.

——, 1984: Boundary layer thermodynamics of a high-plains severe storm. *Mon. Wea. Rev.*, **112**, 2199–2211.

Black, P. G., G. J. Holland and M. D. Powell, 1987: Boundary layer dynamics in Hurricane Kerry 1979, II: Heat and moisture budgets. *J. Atmos. Sci.* (accepted for publication).

Bolton, D., 1980: The computation of equivalent potential temperature. *Mon. Wea. Rev.*, **108**, 1046–1053.

Byers, H. R., 1944: *General Meteorology*, 2nd ed., McGraw-Hill, 645 pp.

Carrier, G. F., A. L. Hammond and O. D. George, 1971: A model of the mature hurricane. *J. Fluid Mech.*, **47**, 145–170.

Charney and Eliassen, 1964: On the growth of the hurricane depression. *J. Atmos. Sci.*, **21**, 68–75.

Emanuel, K. A., 1986: An air–sea interaction theory for tropical cyclones. Part I: Steady state maintenance. *J. Atmos. Sci.*, **43**, 585–604.

Fendell, F. E., 1974: Tropical cyclones. *Advances in Geophysics*, Vol. 17, Academic Press, 2–10.

Frank, W. M., 1977a: The structure and energetics of the tropical cyclone. I: Storm structure. *Mon. Wea. Rev.*, **105**, 1119–1135.

——, 1977b: The structure and energetics of the tropical cyclone. II: Dynamics and energetics. *Mon. Wea. Rev.*, **105**, 1136–1150.

——, 1984: A composite analysis of the core of a mature hurricane. *Mon. Wea. Rev.*, **112**, 2401–2420.

GATE, 1977: *Report of the U.S. GATE Central Program Workshop*, p. 516. Published by NCAR, P.O. Box 3000, Boulder, CO 80307.

Gray, W. M., 1973: Cumulus convection and larger-scale circulations. I: Broadscale and mesoscale considerations. *Mon. Wea. Rev.*, **101**, 839–855.

Hawkins, H. F., and D. T. Rubsam, 1968: Hurricane Hilda, 1964, 2: Structure and budgets of the hurricane on October 1, 1964. *Mon. Wea. Rev.*, **96**, 617–636.

——, and S. M. Imembo, 1976: The structure of a small, intense hurricane, Inez, 1966. *Mon. Wea. Rev.*, **99**, 427–434.

Holland, G. J., and P. G. Black, 1987: Boundary layer dynamics in Hurricane Kerry (1979), I: Mesoscale structure. *J. Atmos. Sci.* (accepted for publication).

Jordan, D. L., 1958: Mean soundings for the West Indies area. *J. Meteor.*, **15**, 91–97.

Jorgensen, D. P., 1984: Mesoscale and convective scale characteristics of mature hurricanes. Part II: Inner core studies of Hurricane Allen (1980). *J. Atmos. Sci.*, **41**, 1287–1311.

Malkus, J. S., 1962: Large-scale interactions. Chapter 4 in *The Sea.* Vol. 1: *Ideas and Observations on Progress in Study of the Sea.* M. N. Hill, I, Ed., Wiley-Interscience, 88–294.

——, and H. Riehl, 1960: On the dynamics and energy transformation in steady-state hurricanes. *Tellus*, **12**, 1–20.

Ooyama, K., 1964: A dynamical model for the study of tropical cyclone development. *Geophys. Inst.*, **4**, 187–198.

——, 1969: Numerical simulation of the life-cycle of tropical cyclones. *J. Atmos. Sci.*, **26**, 3–40.

——, 1982: Conceptual evolution of the theory and modelling of the tropical cyclone. *J. Meteor. Soc. Japan*, **60**, 369–379.

Powell, M. D., 1982: The transition of Hurricane Frederic boundary-layer wind field of the open Gulf of Mexico to landfall. *Mon. Wea. Rev.*, **110**, 1912–1932.

Riehl, H., 1954: *Tropical Meteorology.* McGraw-Hill, 392 pp.

——, 1963: Some relations between wind and thermal structure of steady state hurricanes. *J. Atmos. Sci.*, **20**, 276–287.

——, and J. S. Malkus, 1958: On the heat balance of the equatorial trough zone. *Geophysica*, **6**, 503–537.

——, and ——, 1961: Some aspects of Hurricane Daisy, 1958. *Tellus*, **13**, 181–213.

——, and J. Simpson, 1979: The heat balance of the equatorial trough zone, revisited. *Contrib. Atmos. Phys.*, **52**, 287–305.

Rodgers, E. B., R. A. Mack and A. F. Hasler, 1983: A satellite stereoscopic technique to estimate tropical cyclone intensity. *Mon. Wea. Rev.*, **111**, 1599–1610.

Simpson, R. H., 1978: On the computation of equivalent potential temperature. *Mon. Wea. Rev.*, **106**, 124–130.